Heliyon 9 (2023) e22187

Contents lists available at ScienceDirect

Heliyon

journal homepage: www.cell.com/heliyon

Spectroscopic properties (FT-IR, NMR and UV) and DFT studies of amodiaquine

Pélagie Manwal A Mekoung [a,b,c], Alhadji Malloum [e,f], Munusamy Govindarajan [g,h], Rose Ngono Mballa [c,d], Issofa Patouossa [a], Auguste Abouem A Zintchem [b], Charles P.N. Nanseu [a], Ibrahim N. Mbouombouo [b,i,*]

[a] Department of Inorganic Chemistry, Faculty of Science, University of Yaoundé I, P.O. Box 812 Yaoundé, Cameroon
[b] Computational Chemistry Laboratory, Department of Chemistry, Higher Teacher Training College, University of Yaoundé I, P. O. Box 47 Yaoundé, Cameroon
[c] National Drug Quality Control and Valuation Laboratory, P.O. Box 12216 Yaoundé, Cameroon
[d] Department of pharmacology and traditional medicine, FMSB, University of Yaoundé I, P. O. Box 1364 Yaoundé, Cameroon
[e] Department of Physics, Faculty of Science, University of Maroua, P.O. Box 46 Maroua, Cameroon
[f] Department of Chemistry, University of the Free State, P. O. Box 339, Bloemfontein 9300, South Africa
[g] Department of Physics, Avvivayar Government College for Women, Karaikal, Puducherry, India
[h] Arrignar Anna Govermnet Arts and Science College, Karaikal, Puducherry, India
[i] Department of Applied Chemistry, Faculty of Science, University of Ebolowa, PO. Box 812 Ebolowa, Cameroon

ARTICLE INFO

Keywords:
Amodiaquine
FT-IR
NMR
UV
Thermodynamic indicators
DFT
Reactivity descriptors
TD-DFT

ABSTRACT

Amodiaquine (AQ) was synthesized by a condensation reaction and characterized by experimental FT-IR, ^{1}H and ^{13}C nuclear magnetic resonance (NMR) and UV spectroscopies. In the present work, Density Functional Theory (DFT) calculations.

The structural and spectroscopic (FT-IR, ^{1}H and ^{13}C NMR and UV) data of amodiaquine molecule in ground state have been investigated by using Density Functional Theory (DFT). The calculations have been performed at the using B3LYP method with 6–311++G(d,p) and 6–311++G(2d, p) basis sets theory level were performed, first, to confirm its structure, then to explain its reactive nature through its molecular properties such as natural charges, local and global reactivity descriptors or natural bond orbital (NBO). Afterwards, the calculated properties were compared with experimental results. The ^{1}H and ^{13}C NMR chemical shifts were calculated by using the gauge-independent atomic orbital (GIAO) method, while the electronic UV–Vis spectrum is predicted using the time-dependent density functional theory (TD-DFT). Globally, the computerized results showed good agreement close similarity with the experimental values. The molecular properties such as natural charges, local and global reactivity descriptors, molecular electrostatic potential (MEP), natural bond orbital (NBO) of title molecule were calculated insights into the stability, reactivity and reactive sites on the molecule.

The calculated energy band gap (E_{LUMO}-E_{HOMO}) value of AQ was found to be 4.09 eV suggesting that it could be considered as a hard molecule with high stability, supported by global reactivity descriptors. Molecular electrostatic potential (MEP) analysis revealed heteroatoms (oxygen and nitrogen) as the most putative nucleophilic sites when hydrogen atoms to which they

* Corresponding author.Computational Chemistry Laboratory, Department of Chemistry, Higher Teacher Training College, University of Yaoundé I, P. O. Box 47 Yaoundé, Cameroon
E-mail address: indassa@yahoo.fr (I.N. Mbouombouo).

https://doi.org/10.1016/j.heliyon.2023.e22187
Received 6 August 2023; Received in revised form 3 November 2023; Accepted 6 November 2023
Available online 22 November 2023

are linked appear as electrophilic sites. The potential use of amodiaquine as non-linear optical (NLO) material and its thermodynamic indicators have also been assessed.

1. Introduction

Quinolines are considered as one of the most attractive and versatile class of organic compounds because of their fascinating pharmacological activities such as antibacterial [1], anticancer [2], antitubercularosis [3], antiviral [4], antileishmanial [5,6], anti-inflammatory [7], antimalarial [8] among others. Amodiaquine (AQ), 4-[(7-chloro-4-quinolinyl)amino]-2-[(diethylamino) methyl] phenol (see Fig. 1 with atom numbering), a Mannich base quinoline is synthesized for the first first time in 1940(s) by Burkhalter and co-workers [9]. It is a 4-aminoquinoline similar to chloroquine® in structure and activity, and it has been widely used in the past to treat and prevent malaria. Because of serious toxicity associated with use as prophylaxis, it was withdrawn by the World Health Organisation (WHO) from the list of drugs involved in the treatment of malaria [10,11], and then re-introduced in 21st century as combination with other antimalarial drugs like artesunate® [12–14] and pyrimethamine-sulfadoxine® [15–17], especially in Africa. Many experimental and theoretical studies, have been carried out to characterize this organic compound, including X-Ray powder diffraction (XRD) [18,19] nuclear magnetic resonance (NMR) [20], Fourier transformed infrared spectroscopy (FT-IR) and UV spectrophotometry for analytical techniques [21–23]. Because of their reasonable accuracy, computational efficiency and broad applicability to different molecular systems, DFT calculations provide a better description of molecular properties [24,25].Literature review reveals that very few studies using DFT calculations have been performed. The molecular geometry and natural charge distribution of AQ have been reported at the B3LYP/6-31G(d,p) level of theory by A. Semeniuk et al. [18].M. Hagar exposed DFT calculations and molecular docking of AQ as with regard to COVID 19 [26].Arguelho et al. worked on electrochemical and theoretical evaluation of the interaction between DNA and AQ [27].Theoretical study of the adsorption process of AQ into acrylamide-base hydrogel model using DFT methods was presented by Cortes et al. [28].To the best of our knowledge, spectroscopic, optical and thermodynamic properties of AQ have not been previously studied. To highlightening the characteristics responsible for the biological activity it is crucial to give a more complete description of molecular motion, vibrational, electronic and thermodynamic properties at the quantum scale because these properties are very useful in pharmacology and drug design [29,30]. The main purpose of this research work is to study IR, UV and NMR of AQ molecule using DFT calculations at B3LYP/6–311++G(d,p) and sometimes at B3LYP/6–311++G(2d,p) levels of theory. Furthermore, the natural bond orbital (NBO) analysis, natural charges analysis, molecular electrostatic potential (MEP), local and global reactivity descriptors, Non-Linear optical (NLO), and thermodynamic properties were also provided.

2. Materials and methods

2.1. Experimental details

The pure sample of AQ was obtained from International Chemical Reference Substance (ICRS) Company (in Sweden). The infrared spectrum of title compound were was recorded in the region 4000-400 cm^{-1} using the spectrophotometer with KBr pellet technique

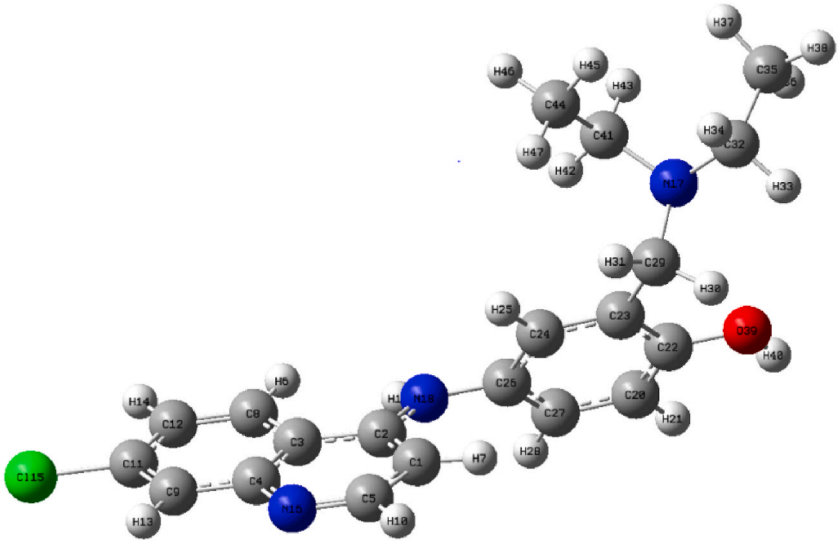

Fig. 1. Optimized geometry of AQ at the B3LYP/6–311++G(d,p) level of the theory.

(solid phase). Absorption spectra were determined on PerkinElmer UV–Vis spectrometer.The sample was dissolved in the water deuteride (D_2O) solvent. The ^{1}H and ^{13}C NMR spectra were recorded on a Bruker Advance (600 MHz for ^{1}H and 125 MHz ^{13}C) NMR spectrometer using tetramethylsilane (TMS) as the internal standard.

2.2. Computational details

The GaussView program 5.0 [31] was utilized used to build the initial structure of AQ molecule. There After which molecular geometry optimizations were carried out in gas phase with the DFT method using the Gaussian 16 program [32]. Results were analyzed with GaussView program 5.0 [31] and GaussSum program [33]. To perform the assignments, potential energy distribution (PED) is calculated using VEDA program [34]. The optimal geometries were verified on minima conditions of frequencies amongst which no imaginary values was were observed. All our calculations were performed using the DFT functional, B3LYP (Becke's three parameter Lee-Yang-Parr) and the 6–311++G(d,p)basis set [29,30].The DFT method tends to overestimate the fundamental modes; therefore scalling factor (0.967 [35,36]) has to be used for to obtaining a considerably better agreement with experimental data. The ultraviolet visible spectrum was predicted in gas phase and in aqueous solution by using time-dependant DFT (TD-DFT) calculations. NMR chemical shifts were calculated with Gauge including atomic orbital (GIAO) method [37,38], using B3LYP/6–311++G(2d,p) level of theory. These spectrumsa were compared with the experimental ones. Furthermore several properties like frontier molecular orbitals (FMOs), energy gap, reactivity descriptors, NBO, natural charges, MEP, NLO and thermodynamic properties were also theoretically investigated.

3. Results and discussion

3.1. Molecular geometry

The molecular structure of AQ was fully optimized in gas phase at B3LYP/6–311++G(d, p) level of the theory, as illustrated in Fig. 1. The results of the selected optimized structure parameters (bond lengths and bond angles) were compared with their corresponding experimental values [18] in Table 1. The C–N bond lengths were calculated from 1.317 Å to 1.467 Å in the same basis set. The three bond lengths C29–N17, C41–N17 and C26–N18 disclose higher values, at 1.466, 1.467 and 1.421 Å, respectively. The bonds with N17 are the highest Here, C41–N17 is the highest among the values of all C–N bonds, due to sp3 hybridation of the atoms. The experimental bond angle In bond angles values, the angle C2–N18–C26 is 125.9°, the highest value slightly higher than the ~120° value corresponding to angles with an sp^2 central atom; the free rotation around the N18–C26 bond, hence σ-properties, could justify that 125.9°value. The correlation coefficients (R^2) between experimental and theoretical values were 0.956 for bond lengths and 0.930 for bond angles. There are only minor deviations between the theoretical and experimental geometrical parameters. Such deviations can be ascribed to the differences in the molecular environment [39]. The experimental X-ray diffraction analysis were carried out in the crystalline phase whereas the theoretical calculation was carried out in the gas phase.

Table 1
Selected theoretical values of geometrical parameters of AQ.

Geometric parameters	**Experimental values**[a]	B3LYP/6–311++G (d, p)
Bond length (Å)		
C2–N18	1.369(3)	1.381
C4–N16	1.369(3)	1.363
C5–N16	1.320(3)	1.317
C9–C11	1.359 (4)	1.371
C11–C12	1.397(4)	1.410
C29–N17	1.473(4)	1.466
C41–N17	1.485(4)	1.467
C26–N18	1.418(3)	1.421
C20–C22	1.377(4)	1.393
C22–C23	1.395(4)	1.406
R[b]	/	0.956
Bond angles (°)		
C9–C11–C12	121.7(2)	121.6
C4–N16–C5	116.0 (2)	116.5
C29–N17–C41	112.1(3)	114.1
C2–N18–C26	125.9(2)	126.1
C2–N18–H19	118(2)	116.1
C26–N18–H19	116(2)	115.2
C20–C22–C23	120.2(2)	120.3
R^2	/	0.930

For numbering of atoms refer to Fig. 1.
[a] See reference [18].
[b] R^2 represents *the correlation coefficient between experimental and theoretical data.*

Table 2
Experimental FT-IR and calculated vibrational frequencies in cm^{-1} for AQ.

Exp. FT-IR (cm^{-1})	B3LYP/6–311++G(d.p)			Vibrational assignments
	Unscaled	Scaled	$^{a}I_{IR}$	
3406 m	3838	3711	87,14	(O–H)
3348 m	3633	3513	22,80	(N–H)
3170 m	3213	3107	0,57	ν(C–H) R_1
	3209	3103	5,57	ν(C–H) R_1
	3206	3100	2,74	ν(C–H) R_1
	3176	3071	5,90	ν(C–H) R_2
	3175	3070	5,99	ν(C–H) R_2
	3171	3066	8,92	ν(C–H) R_1
	3150	3046	21,07	ν(C–H) R_2
3000	3135	3032	26,15	ν(C–H) R_1
	3100	2998	50,19	$\nu_{as}CH_3$ (C35)
	3097	2995	34,81	$\nu_{as}CH_3$ (C44)
	3092	2990	56,35	$\nu_{as}CH_3$ (C35)
	3087	2985	29,21	$\nu_{s}CH_3$ (C44)
	3071	2970	12,53	(C29–H30)
	3067	2966	7,53	$\nu_{as}CH_2$ (C41)
	3047	2946	7,64	ν(C–H) D
	3042	2942	29,47	$\nu_{s}CH_2$ (C41)
2937w	3030	2930	23,86	$\nu_{s}CH_3$ (C35)
	3028	2928	23,91	$\nu_{s}CH_3$ (C44)
	2936	2839	72,23	ν(C–H) D
	2905	2809	85,92	ν(C–H) D
1586s	1652	1597	14,67	ν(CC) R_2
	1643	1589	102,03	ν(CC) R_1
	1635	1581	5,23	ν(CC) R_2
	1621	1568	51,93	ν(CC) R_1
	1600	1547	327,49	ν(CC) R_1
1508w	1555	1504	265,59	β(HNC) (N18)
	1536	1485	134,36	β(HCC) R_2
	1520	1470	0,95	βCH_2 (C32)
	1509	1459	17,88	βCH_2 (C32)
	1507	1457	2,56	βCH_2 (C32)
	1504	1454	2,95	$\delta_{as}CH_3$ (C44)
	1502	1452	2,54	βCH_3 (C44)
	1498	1449	4,73	βCH_3 (C35)
	1487	1438	1,76	βCH_2 (C41)
	1484	1435	3,21	βCH_2 (C29)
	1474	1425	19,30	β(HCN) R_1
1445s	1463	1415	253,13	ν(CC) R_2
1364w	1429	1382	9,39	τ(HCNC) D
	1405	1359	7,72	wCH_3 (C35)
	1404	1358	27,44	wCH_3 (C44)
	1400	1354	100,23	(N–C) R_1
	1389	1343	43,04	$twCH_2$ (C41)
	1380	1334	6,86	wCH_2 (C41)
	1371	1326	38,39	ν(CC) R_1
	1356	1311	16,90	β(HOC)
	1353	1308	138,80	τ(HCCC) (C29)
	1349	1304	38,99	$twCH_2$ (C41)
	1337	1293	31,47	$twCH_2$ (C32)
	1317	1274	33,34	$twCH_2$ (C32)
1209 m	1289	1246	14,78	ν(OC)
	1281	1239	50,44	τ(HCCC) (C29)
	1266	1224	34,17	β(HCC) R_1
	1261	1219	2,46	β(HCC) R_1
	1225	1185	13,82	τ(HCCN) D
	1221	1181	15,02	ν(NC) R_1
1163w	1202	1162	87,33	β(HOC)
	1194	1155	20,33	$twCH_2$ (C29)
	1187	1148	17,64	β(HCC) R_1
	1177	1138	8,30	β(HCC) R_2
	1142	1104	9,78	τ(HCNC) D
	1130	1093	1,21	β(HCC) R_1
1055w	1122	1085	107,20	β(HCC) R_2
	1092	1056	6,85	τ(HCCN) D
	1089	1053	37,05	ν(CC) R_1
1047w	1070	1035	33,35	ν(NC) D

(*continued on next page*)

Table 2 (*continued*)

Exp. FT-IR (cm^{-1})	B3LYP/6–311++G(d.p)			Vibrational assignments
	Unscaled	Scaled	$^{a}I_{IR}$	
	1066	1031	28,71	ν(CC) R_1
	1053	1018	17,44	ν(CC) D
	1016	982	5,85	ν(CC) D, β(HCC) (C29)
	983	951	2,02	τ(HCNC) R_2
	971	939	15,40	ν(CC) D
	964	932	4,34	ν(CC) R_2
	955	923	0,32	τ(HCCC) R_1
	935	904	4,88	τ(HCCN) R_2
	928	897	11,98	τ(HCCN) R_1
	911	881	35,81	β(CCC) R_1
	907	877	22,49	ν(CC) D
	906	876	12,26	τ(HCCC) R_1
839w	864	835	79,39	β(NCC) R_1
	844	816	18,54	τ(HCCC) R_1
	836	808	23,91	τ(HCCC) R_1
	823	796	7,78	τ(HCCC) R_1
	819	792	8,82	τ(HCCN) D
755w	797	771	6,69	β(CCC) R_2
	788	762	11,26	τ(HCCC) R_1
	781	755	20,00	τ(HCCN) D
	778	752	13,54	β(CCC) R_1
	771	746	7,53	τ(CCNC) R_2
	765	740	1,49	β(CCC) R_2
	738	714	1,11	τ(CCCC) R_2
650w	677	655	6,82	ν(CC) R_2, β(CCC) R_2
	653	631	7,92	τ(CCCC) R_1
	632	611	2,82	τ(CCCN) (N18)
	605	585	5,62	β(CNC) R_2
	589	570	5,90	τ_o(NCCC) (N18)
542vw	564	545	11,60	β(CCC) R_2
	530	513	16,83	β(CCC) R_1, β(NCC) (N18)
	514	497	4,99	τ_o(CCCC) R_2
	512	495	7,14	τ_o(OCCC) R_1
	487	471	7,13	β(OCC)
	482	466	1,46	β(CCN) D
	461	446	7,57	β(CCC) R_1
	449	434	2,57	β(CNC) D
	437	423	18,07	τ(CCCC) R_1
	388	375	10,16	τ(CCCC) R_2
	378	366	6,95	ν(ClC) R_2
	366	354	11,16	β(CCN) D
	355	343	22,42	τ(CCCC) R_2
	338	327	110,35	τ(HNCC) (N18)
	320	309	54,41	τ(HOCC)
	316	306	24,15	β(CCC) (C29)
	288	278	0,54	τ(HCCN) D
	268	259	1,41	τ_o(ClCCC) R_2
	247	239	2,56	β(ClCC) R_2
	238	230	0,41	β(ClCC) R_2
	233	225	0,30	τ(CCCN) (N18)
	226	219	2,36	β(CNC) D
	202	195	0,82	τ_o(CCCN) D
	162	157	0,21	τ(CCCC) R_1
	137	132	0,51	β(CCN) (N18)
	128	124	0,35	τ(CCNC) D
	120	116	2,01	τ(CNCC) R_1
	95	92	0,97	τ(CCNC) D
	81	78	0,48	τ(CCCC) R_1
	70	68	0,37	τ(CCNC) D
	50	48	0,16	β(CNC) (N18)
	40	39	0,24	τ(CNCC) D
	31	30	0,19	τ(CNCC) D
	19	18	0,59	τ(CNCC) (N18)
	14	14	0,17	τ(CCNC) (N18)

vs, very strong; s, strong; m, medium; w, weak; vw, very weak; $^{a}I_{IR}$: IR intensities (Km/Mol), ν: stretching; β: deformation in the plane; δ: deformation; w: wagging; tw: twisting; τ: torsion; R_1: quinolone ring; R_2: phenyl ring; D: diethylamino)methyl.

3.2. Vibrational assignments

Molecular structure of AQ, consisting of 47 atoms showing 135 vibrational modes, belongs to C_1 symmetry point group. The goal of the vibrational analysis is to find vibrational modes connected with specific molecular structure of calculated compound. The experimental and calculated vibrational frequencies of the title molecule with their tentative assignments are presented in Table 2. The experimental FT-IR spectrum was recorded in a solid state using reflectance mode. A comparison of experimental spectrums of AQ in solid phase with the corresponding prediction in gas phase by using B3LYP/6–311++G(d,p) method can be seen in Fig. 2. From results we observed that the calculated wavenumbers are higher than the corresponding experimental values due to: 1-difference in physical states; 2-discard of anharmonicity present in real system.

3.2.1. O–H vibration

O–H vibrations of phenols generally appear at roughly 3500 cm^{-1} [40] with broad band. In the present study the stretching vibration of hydroxyl group of AQ was observed in IR spectrum at 3406 $cm^{-1}$and predicted scaled value is 3711 cm^{-1}.The in-plane bending vibration of O–H is observed at 1163 $cm^{-1}$and the calculated value is 1162 1185 cm^{-1}. They are well coincided perfectly well with the PED values.

3.2.2. N–H vibration

N–H vibrations are expected in the range 3500-3300 cm^{-1} [41,42]. In the present case DFT calculations provided value at 3513 cm^{-1} while the IR peak is experimentally observed at 3348 cm^{-1}. The N–H in-plane bending vibrations usually occur in the region 1650-1580 cm^{-1} [43]. The N–H in-plane bending vibration is observed at 1508 1445 cm^{-1} and the calculated value is 1504 1470 cm^{-1}.

3.2.3. C–H vibrations

The aromatic structure shows the presence of = C–H stretching vibrations around 3100-3000 cm^{-1} [41,44]. In this work, the = C–H stretching vibrations of the AQ ring appear in the IR spectrum at 3000 cm^{-1} while simulated ones at 3107, 3103, 3100, 3071, 3066, 3046 and 3032 cm^{-1}. Because of the confusion (sometimes strongly) with various C═C ring vibrations, many bands in the 1600-1000 cm^{-1} are involved in-plane C-H bending vibrations [45,46]. The C–H in plane bending vibrations of phenyl rings were observed at

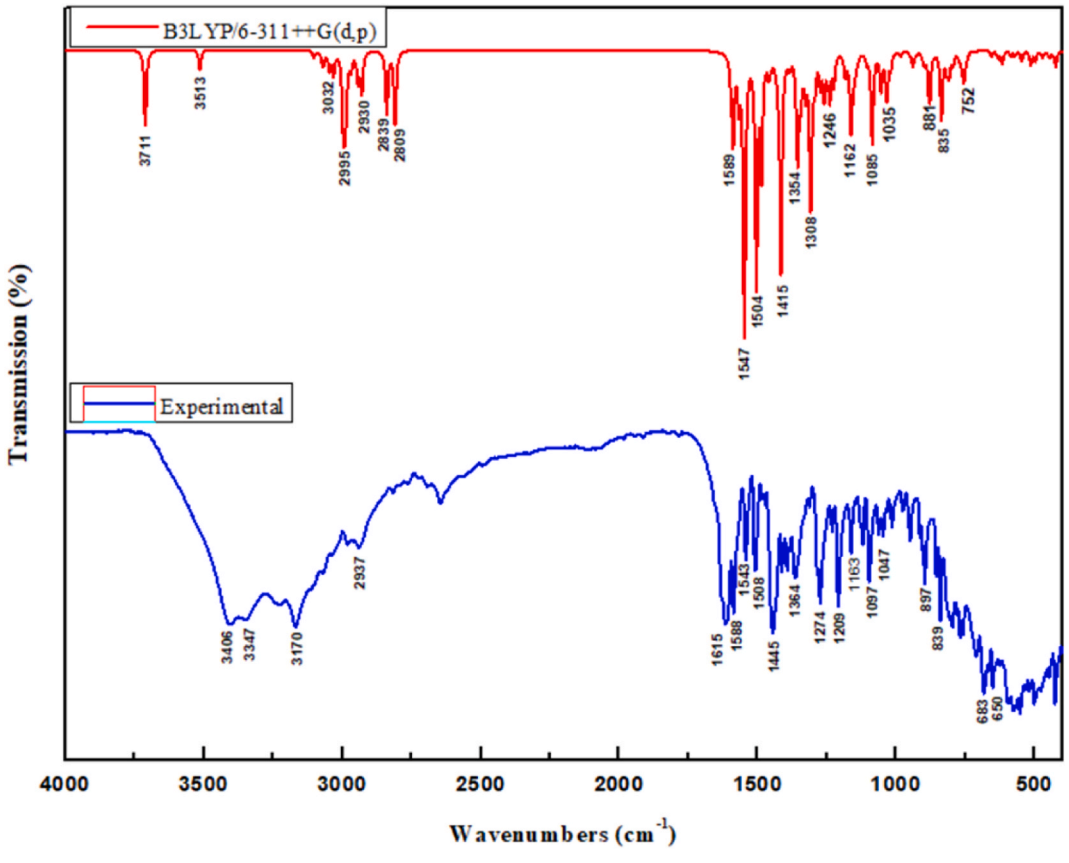

Fig. 2. Experimental and simulated FT-IR spectra of AQ.

~1055 cm^{-1} (FTIR spectrum), while the calculated values appeared at 1485, 1224, 1219, 1148, 1138 and 1085 cm^{-1}.

3.2.4. CH_2 and CH_3 vibrations

The asymmetric methylene stretching vibrations are typically observed in the range of 3000-2900 cm–1 while the symmetric ones are observed at the interval 2900-2800 cm–1 [47,48]. There were five fundamental vibrations belonging to CH_2 modes in this molecule (asymmetric stretching, symmetric stretching, in-plane bending, twisting and wagging vibrations). These vibrations were predicted at 2966 cm–1 (*asym.*), 2942 cm–1 (*sym.*), 1470, 1459, 1457, 1438 and 1435 cm–1 (in plane bending), 1304, 1293, 1274 and 1155 (twist.) and 1380 cm–1 (wag.).

The vibrations of the CH_3 group, are expected in the range of 2900 3050-2900 cm^{-1} [49,50]. The calculated asymmetric stretching modes of the methyl group were found to be: 2998, 2995, and 2990 cm^{-1} while, the symmetric modes were at 2985, 2930 and 2928 cm^{-1}. Experimental bands were observed at 2937 cm^{-1} in the IR spectrum. The CH_3 symmetric stretching vibrations were found after calculations at 2930 cm^{-1}at a value very closed to experimental one (2930 cm^{-1}). The predicted wavenumbers at 1454, 1452 and 1449 cm^{-1} were assigned as CH_3 bending vibrations while wagging wCH_3 of AQ were identified at 1359 and 1358 cm^{-1}.

3.2.5. C═C and C═N vibrations

Generally C═C stretching vibrations in aromatic compounds display bands between 1430 and 1650 and 1430 cm^{-1} [51,52]. In this work, experimental C═C stretching bands were observed at 1615, 1588, 1543, 1550 and 1445 1395 cm^{-1} and they were computerized to be 1597, 1589, 1581, 1568, 1547 and 1415 cm^{-1}, respectively.

Because of the mixing of several bands, the identification of C═N vibrations is a very difficult task. Silverstein assigned C═N and C–N absorption in the region 1382–1266 cm^{-1} and 1250-1020 cm^{-1}, respectively [53]. The bands observed at 1364 cm^{-1} in FT-IR spectrum have been assigned to C═N. The theoretically calculated latter value of C═N is observed at 1354 1382 cm^{-1} while C–N stretching were observed at 1047 cm^{-1} in FT-IR and predicted at 1035 cm^{-1} by B3LYP/6–311++G(d,p) method. The CCN (quinoline ring) in plane bending is observed at 839 cm^{-1} in FT-IR and theoretically computed scaled wave number at 835 cm^{-1}.

3.2.6. C–O vibrations

The C–O stretching vibrations of phenols were observed between 1300 and 1200 cm^{-1} in the literature [54,55]. The experimental C_{22}–O_{39} stretching vibration was observed at 1209 cm^{-1} in IR spectra of AQ. Here, the C_{22}–O_{39} (H) stretching mode given at 1209 cm^{-1} and the computed mode was found at 1246 cm^{-1}.

3.3. ^{1}H and ^{13}C NMR data

The NMR is particularly useful in determining the structure of organic and inorganic compound in solution by revealing hydrogen and carbon skeleton. In order to provide a definite assignment and analysis of ^{1}H and ^{13}C NMR spectra, the Gauge Including Atomic Orbital (GIAO) ^{1}H and ^{13}C chemical shifts calculations of AQ were performed. The IEFPCM and universal solvation methods were employed in the optimization of AQ in solution because the solvent effects are considered [56,57]. The obtained data have been compared with experimental ones (see Table 3 and Table 4). Figs. 3 and 4 depicts the experimental ^{1}H and ^{13}C NMR spectra of AQ, respectively. The correlation graph between the experimental and calculated chemical shifts for ^{1}H and ^{13}C NMR are shown in Fig. 5.

Table 3
The experimental and theoretical ^{1}H NMR chemical shifts for AQ.

Atoms	Experimental	**B3LYP/6–311++(2d,p)**
H10	8.5	8.76
H13	/	8.28
H6	/	8.18
H14	7.9	7.79
H25	7.6	7.48
H28	7.5	7.23
H7	7.2	7.02
H21	/	7.00
H19	6.8	6.65
H40	4.7	4.59
H30	/	3.77
H31	3.4	3.71
H34	/	3.13
H43	/	2.79
H33	/	2.68
H42	/	2.62
H37	1.5	1.32
H47	/	1.11
H38	/	1.07
H45	/	0.91
H36	/	0.90
H46	/	0.18

Chemical shifts of O–H (H19) and N–H (H40) group was observed at 6.8 ppm and 4.7 ppm, respectively, while they were predicted at 6.65 ppm and 4.59 ppm using B3LYP/6–311++ (2d, p). As seen at Fig. 4, there are correlations between experimental and calculated ^{1}H NMR results and the corresponding R^2 values were found as 0.992.

The ^{13}C NMR spectra of AQ showed the chemical shifts of C–OH (C22) are predicted at 160.3 ppm at B3LYP/6–311++ (2d, p). The correlation values ($R^2 = 0.992$) for ^{1}H NMR and ($R^2 = 0.999$) for ^{13}C NMR show that there is a perfect agreement similarity between the experimental and theoretical chemical shifts.

3.4. Frontier molecular orbitals (FMO) (HOMO-LUMO) and UV–Vis analysis

The energies of HOMO (E_H) and LUMO (E_L) characterize the ability of a molecule to donate and accept electrons, respectively [58–60]. These orbitals are named as frontier molecular orbitals (FMOs).The difference between E_H and E_L is called energy gap (Δ_{EG}). The energy gap of HOMO–LUMO explains the eventual charge transfer interaction [61] within the molecule and the stability of a molecule, influencing its the biological activity of the molecule. From FMOs calculations, the kinetic stability, UV spectra and chemical reactivity and chemical hardness-softness were predicted. According to the HSAB (hard and soft acids and bases) principle, a molecule with a high HOMO-LUMO energy gap is less reactive and can be considered as a hard molecule [62–64]. The HOMO, LUMO, HOMO-1 and LUMO+1 orbitals of AQ were calculated with Gaussian 16 program using B3LYP/6–311++G(d, p).These energies are illustrated in Fig. 5 and their values were summarized in Table 4. The value of the energy separation between the HOMO and LUMO is 4.09 eV. This result probably suggested that it is a hard molecule.

In addition to the frontier orbitals, other orbitals are involved in the development of the UV–Vis spectrum. This is the case for the orbital preceding the HOMO, whose energy will be noted as E_{H-1}, and the orbital following the LUMO, noted as E_{L+1}, whose values have been obtained in Table 4.

3.5. UV–Vis spectra analysis

Electronic transitions are usually classified according to the orbitals engaged or to specific parts of the molecule involved. Common types of electronic transitions in organic compounds are $n\rightarrow\sigma^*$, $n\rightarrow\pi^*$ and especially (donor)$\rightarrow\pi^*$(acceptor) [63]. In order to understand the electronic transitions of AQ, theoretical calculations ofn electronic absorption spectrum were performed in the ground state and in solution (water) using TD-DFT calculations [48,65] with the B3LYP/6–311++G(d, p) level of theory. The computed properties such as absorption wavelengths (λ), excitation energies (E) and oscillator strengths (f) are shown in Table 5. The theoretical electronic absorption wavelengths values for title molecule are 341.3, 333.9 and 302.0 nm in gas phase and 354.7, 341.4 and 304.1 in water. The experimental value is found to be 342.9 nm. The predicted wavelengths are in good agreement with experiment. This electronic absorption corresponds to the transition from HOMO (H) to LUMO (L) in water and HOMO-1 to LUMO in gas phase; (see transitions in Table 5). It seems most likely that solvation (possibly referring to hydrogen bonds formation) tends to decrease energy gap within the H-1 → L transition, hence the bathochromic effect noticeable from gas phase to water medium. The observed UV–Vis and calculated spectra of AQ molecule are shown in Fig. 6.

Table 4
The experimental and theoretical^{13}C NMR chemical shifts for AQ.

Atoms	Experimental	**B3LYP/6–311++(2d,p)**
C22	/	160.3
C5	/	158.0
C4	/	156.7
C2	/	155.0
C11	148.0	148.4
C26	136.0	136.4
C9	134.0	134.2
C23	132.0	133.0
C24	132.0	132.9
C12	/	129.9
C27	/	128.8
C8	/	126.6
C3	123.0	123.5
C20	119.0	119.7
C1	105	103.6
C29	/	55.3
C32	45.0	50.3
C41	40.0	40.4
C35	/	14.3
C44	/	1.1

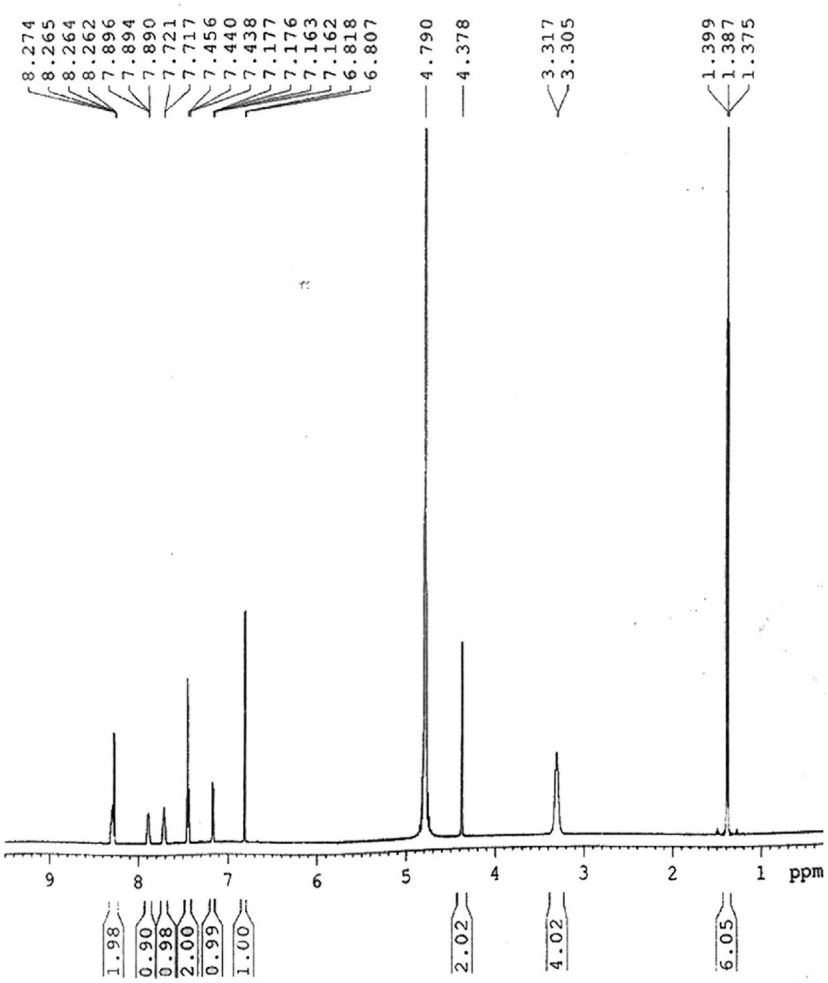

Fig. 3. ^{1}H NMR spectra of AQ.

3.6. Reactivity descriptors

3.6.1. Global reactivity descriptors

Global reactivity descriptors such as ionization potential (IP), electron affinity (EA), chemical hardness (η), softness (S), chemical potential (μ), electrophilicity index (ω) and electronegativity (χ) were calculated using HOMO and LUMO results. All these properties which are defined in Table 6 provide additional informations on the chemical stability of the molecule.

For the title compound, the calculated values of ionization potential, electron affinity, hardness, softness, chemical potential, electrophilicity and electronegativity were 5.81, 1.72, 2.04, 362.46, −3.77, 3.47 and 3.77 eV respectively. Note that the high ionization energy and negative chemical potential (μ) indicate stability of molecule. The electrophilicity (ω) of the AQ molecule is greater than 1.5 eV [66], indicating that it could be classified as strong electrophiles, probably consequent to acidic properties of hydrogen atoms linked to heteroatoms (nitrogen and oxygen) whose free doublets take part to delocalization (like someone of chlorine) with π-electrons of aromatic rings.

3.6.2. Local reactivity descriptors

Some important indicators of reactivity are the Fukui functions (FFs) which provide information on the local site reactivity within the molecule and system, aiming to understand the nature of chemical reactions (nucleophilic and electrophilic behaviours of the molecule). These values correspond to the qualitative descriptors of reactivity of different atoms in the molecule. A study by Ayers and Parr [67] has shown that a larger FF suggests an attack by soft reagents and a smaller FF means an attack by hard reagents. From Mulliken atomic charges of cationic and anionic states, local Fukui functions (f^{+}, f^{-}), and local softness values (s^{+}, s^{-}) were calculated using the following equations:

$$f^{+} = [q(N+1) - q(N)] \text{for nucleophilic attack}$$

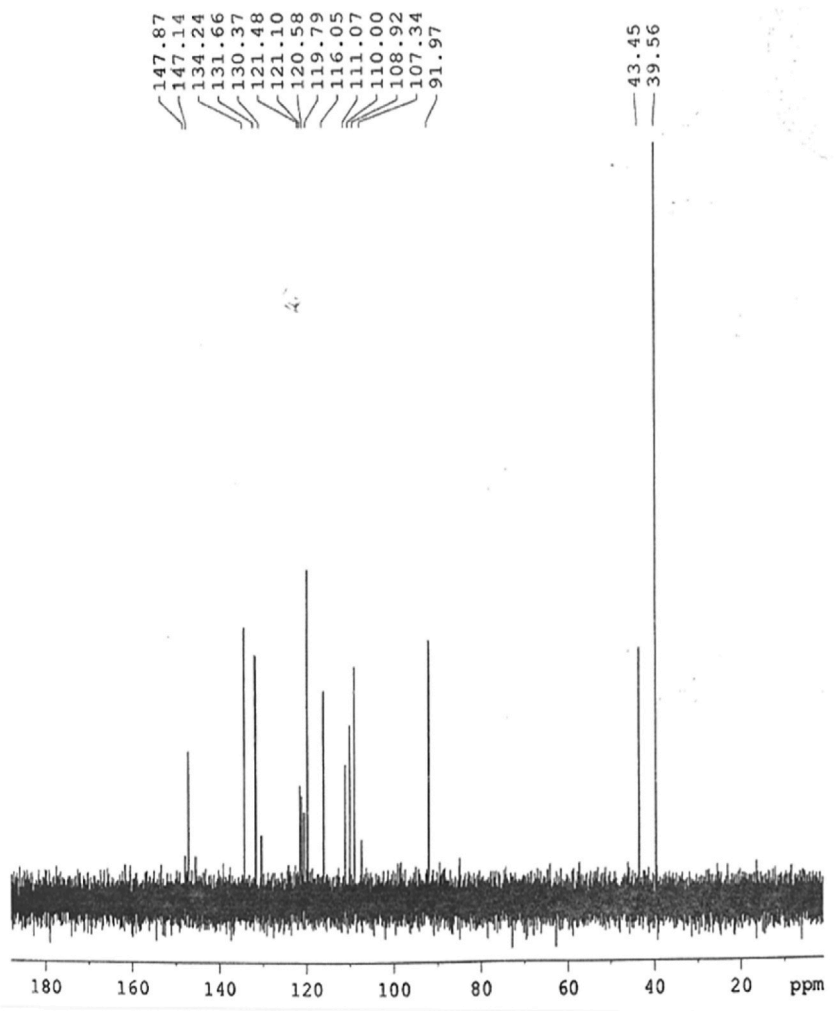

Fig. 4. ^{13}C NMR spectra of AQ.

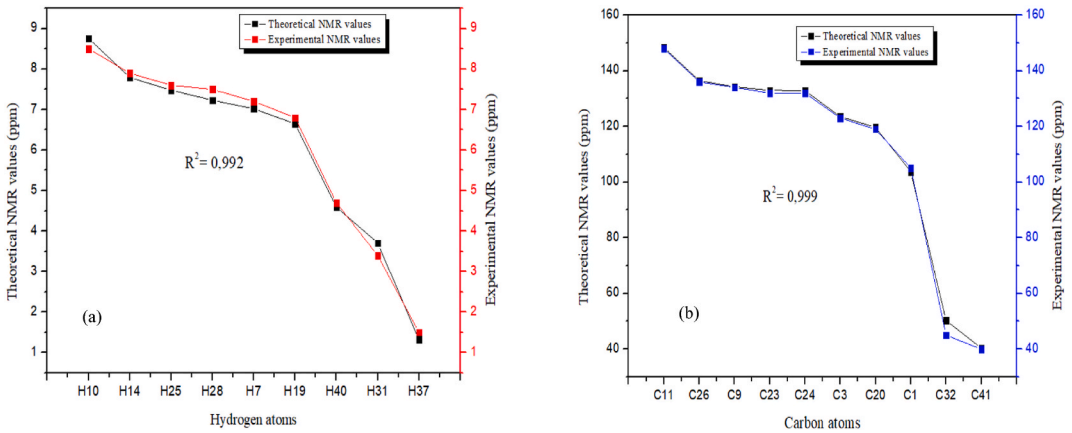

Fig. 5. Correlation graph between experimental and calculated ^{1}H NMR (a) and ^{13}C NMR (b) chemical shift using B3LYP/6–311++(2d,p) level.

$f^{-} = [q(N) - q(N-1)]$for electrophilic attack

Table 5
HOMO-LUMO and dipole moment of AQ by B3LYP/6–311++G(d, p) method.

Property	Symbol and formular	B3LYP/6–311++G (d, p)
Electronic energy (a.u)	/	−1475.35
HOMO energy (eV)	E_H	−5.81
LUMO energy (eV)	E_L	−1.72
$\Delta E_{HOMO\text{-}LUMO}$ gap (eV)	$E_G = E_L\text{-}E_H$	4.09
HOMO-1 energy (eV)	$E_{H\text{-}1}$	−5.86
LUMO+1 energy (eV)	E_{L+1}	−1.01
$\Delta E_{HOMO\text{-}1\text{-}LUMO+1}$ gap (eV)	$E_G = E_{L+1}\text{-}E_{H\text{-}1}$	4.86
Dipole moment (Debye)	D	5.96

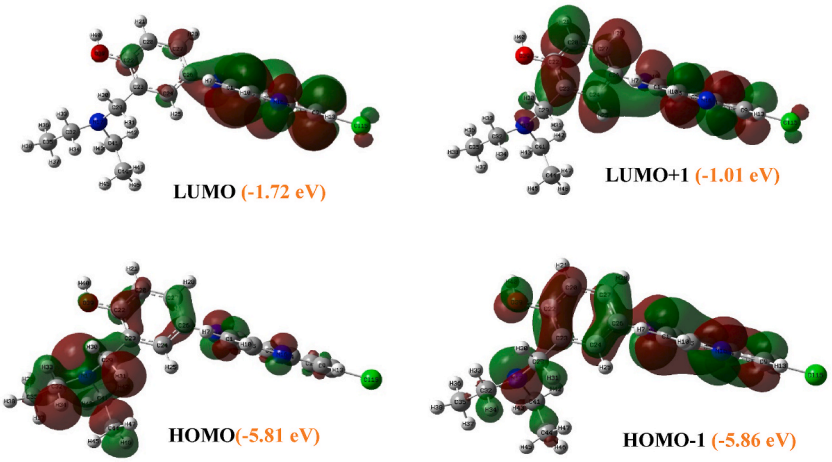

Fig. 6. Atomic orbital compositions of AQ.

$f^0 = 1/2[q(N+1) + q(N-1)]$for radical attack.

Local softness values are calculated using.

$S^+ = sf^+$, $S^- = sf^-$ where + and − signs show nucleophilic and electrophilic attack, respectively with S = 13.32 a.u.

According to DFT/B3LYP/6–311++G(d, p) calculations, Fukui functions and local softness values for selected atomic sites in AQ are listed in Table 7. The relative high values of local reactivity descriptors (f^+, s^+) in Table 7 at Cl15, N16 and N18 indicate nucleophilic sites that these sites are prone to nucleophilic attacks whereas the relative high value of local reactivity descriptors (f^-, s^-) at H21, H40 and H19 indicate electrophilic sites that those sites are more prone to electrophilic attacks. In order to clarify reactivity, dual descriptor (Δf) introduced by Morell et al. [68] was also calculated by:

$$\Delta f(k) = f_k^+ - f_k^-$$

The atomic sites with a higher nucleophilic tendency are those having positive dual descriptor value while those having negative dual descriptor value are the most electrophilic sites [69]. The nitrogen (N16, N18) and oxygen (O39) atoms have the positive dual descriptor indicating possible nucleophilic sites in the drug while hydrogen (H19, H21 and H40) and chlorine (Cl15) atoms have negative dual descriptor indicating possible electrophilic site.

3.7. Molecular electrostatic potential (MEP) analysis

In order to validate the evidence about the reactivity of title compound, MEP was calculated at the B3LYP/6–311++G(d, p) optimized geometry and is shown in Fig. 7. This figure provides a visual representation of the chemically active sites and comparative reactivity of atoms. The potential values increase from red to blue color [70]. Blue colour indicates the strongest attraction and the red colour indicates the strongest repulsion [44]. Regions of negative potential are usually associated with the lone pair of electronegative atoms. The negative electrostatic potential corresponds to an attraction of the proton by the aggregate electron density in the molecule (shades of red), while the positive electrostatic potential corresponds to the repulsion of the proton by the atomic nuclei (shades of blue) [71]. The colour code of MEP map is in the range between −0.06179e (deepest red) to 0.06179e (deepest blue) in our molecule. As can be seen from Fig. 7 the negative electrostatic potential regions (red) were localized on the oxygen (O39) and nitrogen (N16) atoms indicating possible nucleophilic sites for electrophilic attacks. However, positive potential regions (blue) were localized on hydrogen atoms (H40 and H19) around O–H, N–H groups (O39, N18), and indicating possible electrophilic sites for nucleophilic attacks as previously hypothesised. The docking study by M. Hagar et al. [26] reveals that AQ could be a better inhibitor of SARS-CoV-2

Table 6
Experimental and calculated electronic bands of AQ.

Experimental		TD-B3LYP/6–311++G(d,p)							
Water		GAS				Water			
ʎ (nm)	Abs.	ʎ (nm)	E (eV)	f (a.u)	Major/Minor contribs	ʎ (nm)	E (eV)	f (a.u)	Major/Minor contribs
341.9	0.50	341.3	3,63	0.227	H-1- > LUMO (61 %), HOMO- > LUMO (36 %)	354.7	3,50	0.279	H-1- > LUMO (46 %), HOMO- > LUMO (53 %)
		333.9	3,71	0.012	H-1- > LUMO (36 %), HOMO- > LUMO (63 %)	341.4	3,63	0.006	H-1- > LUMO (53 %), HOMO- > LUMO (47 %)
		302.0	4,11	0.012	HOMO- > L+1 (76 %), HOMO- > L+2 (16 %) H-1- > L+2 (5 %)	304.1	4,08	0.008	H-3- > LUMO (11 %), H-1- > L+1 (47 %), HOMO- > L+1 (34 %) H-2- > LUMO (5 %)

Absorption wavelength ʎ (nm), Excitation energies E (eV), Oscillator strengths (f), HOMO (H) and LUMO (L)

Table 7
The calculated HOMO–LUMO energy and Global reactivity descriptor values of AQ using B3LYP/6–311++G (d, p).

Property	Symbol and Formular	B3LYP/6–311++G (d, p)
Ionization potential (eV)	$I = -E_H$	5.81
Electron affinity (eV)	$EA = -E_L$	1.72
Chemical hardness (eV)	$\eta = (E_L\text{-}E_H)/2$	2.04
Global Softness or Chemical reactivity (eV-1)	$S = 1/\eta$	362.46
Chemical potential (eV)	$\mu = (E_L + E_H)/2$	−3.77
Electrophilicity index (eV)	$\omega = \mu^2/2\eta$	3.47
Electronegativity (eV)	$\chi = -\mu$	3.77

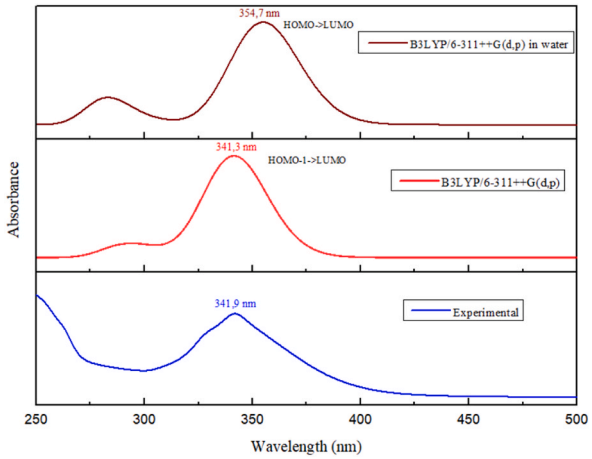

Fig. 7. Experimental and theoretical UV-spectra of AQ.

M^{pro} with binding affinity −7.77 kcal/mol compared to hydroxychloroquine (−6.06 kcal/mol) and remdesivir (−4.96 kcal/mol). AQ interacted with the receptor by different hydrophobic interactions besides three hydrogen bonds with amino acids Leu141, Cys145, and Gln189.

The effective interactions of proteins with the AQ were found on the atoms (N16, N18, and O39) and this could be attributed to the presence of lone pair electrons on these atoms.

3.8. Natural charges analysis

Atomic charges determine many properties of molecular systems. The natural atomic charges of title molecule obtained by natural bond orbital (NBO) analysis are tabulated in Table 8 (atom numbering according to Fig. 1). All carbon atoms are negative, except C2, C4, C5, C22 and C26 that are bonded to electron-withdrawing nitrogen and oxygen atoms, with C2 and C26 bound to N18, C4 and C5 bound to N16 and C22 bound to O39 being the most-positively charged carbon atoms in the molecule, whereas C44 and C35 are the most-negatively charged carbon atoms. All electronegative oxygen and nitrogen atoms have a negative charge, perform as donor atoms, they should endure electrophilic reaction. The oxygen O39 atom is found to exhibit the most negative charge in the molecule due to its electron withdrawing nature. The dominance of red colour in the MEP map around this oxygen atom also confirms this hypothesis. All hydrogen atoms are positive however the most positive charges are localized on hydrogen atoms (H40 and H19) connected to heteroatoms (oxygen O39 and nitrogen N18) because they can be involved in hydrogen bonding.

Table 8
Fukui functions (f^+, f^-) and local softness (s^+, s^-) for selected atomic sites of AQ, using Mulliken population analysis at B3LYP/6–311 G (d, p) level.

N° Atom	N	N+1	N-1	f^+	f^-	Δf	f^0	s^-	s^+
Cl15	0.465654	0.549051	0.357426	0.083397	0.108228	−0.024831	0.0958125	1.44159696	1.11084804
N16	0.021326	0.100847	−0.035008	0.079521	0.056334	0.023187	0.0679275	0.75036888	1.05921972
N18	0.195469	0.254541	0.169666	0.059072	0.025803	0.033269	0.0424375	0.34369596	0.78683904
H19	0.21189	0.241657	0.081163	0.029767	0.130727	−0.10096	0.080247	1.74128364	0.39649644
H21	0.145912	0.189003	−0.288558	0.043091	0.43447	−0.391379	0.2387805	5.7871404	0.57397212
O39	−0.202845	−0.170546	−0.23336	0.032299	0.030515	0.001784	0.031407	0.4064598	0.43022268
H40	0.268432	0.288778	0.013485	0.020346	0.254947	−0.234601	0.1376465	3.39589404	0.27100872

3.9. Natural bond orbital (NBO) analysis

The natural bond orbital (NBO) calculations were performed using NBO program [72] as implemented in Gaussian 16 package at the DFT/B3LYP level under 6–311++G(d, p) basis set in order to understand second order interactions between filled Lewis-type (bond or lone pair) and vacant (anti-bond Rydberg) orbital spaces, which provide an evidence for the charge transfer interactions arising within the molecular systems. This interaction was deduced from the second-order Fock matrix [73,74], as follows:

$$E(2)= \Delta E_{ij} = q\frac{(F_{ij})^2}{(E_j - E_i)}$$

Where E(2) is stabilization energy with the delocalization for each donor (i) and acceptor (j), q is the donor orbital occupancy, E_i and E_j are diagonal elements and F_{ij} is the off diagonal NBO Fock matrix element [75]. The larger E(2) value the more intensive is the interaction between electron donors and acceptor i.e. the more donation tendency from electron donors to electron acceptors and the greater the extent of conjugation of the whole system [40]. Delocalization of electron density between occupied Lewis type (bond or lone pair) NBO orbitals and formally unoccupied (antibond or Rydgberg) non-Lewis NBO orbital's corresponding to a stabilizing donor-acceptor interaction. Table 9 shows the most important interactions between donor and acceptor elements of title molecule in supporting information (SI). The results of the natural bond orbital analysis show that the strong stabilization energy occurs at 92845.91 kcal.mol^{-1}due to BD(1) O39–H40 to RY*(1) C24 interaction. This highest activity around the phenyl ring can induce the large biological properties of AQ. The energy contribution of BD(1) C24–H25 -> RY*(7) C26, BD(1) O39–H40 -> RY*(7) C41 and BD(1) C22–O39 ->RY*(1) C31 are 65072.77, 59862.22 and 52218.60 kcal mol^{-1}, respectively.

3.10. NLO properties

The NLO properties were performed to study the influence of the molecular structure on the polarizations and hyperpolarizations of title molecule due to their suitability for optoelectronic and photonic applications [76]. NLO analysis deals with the interaction of electromagnetic fields in various materials to produce new fields, altered in wavenumber phase or other physical properties [77,78]. The first hyperpolarizability (β), dipole moment (μ), polarizability (α) and anisotropy of polarizability (Δα) of AQ were calculated using B3LYP/6–311++G(d, p) level using Gaussian 16 program package. The x,y,z components of μ, α, and β were used to extract the values of interest using the following equations [79].

$$\beta_x = \beta_{xxx} + \beta_{xyy} + \beta_{xzz}\ \beta_y = \beta_{yyy} + \beta_{xxy} + \beta_{yzz}\ \beta_z = \beta_{zzz} + \beta_{xxz} + \beta_{yyz}$$

$$\beta = \sqrt{\beta_x^2 + \beta_y^2 + \beta_z^2}\ \mu = \sqrt{\mu_x^2 + \mu_y^2 + \mu_z^2}\ \alpha = \frac{\alpha_{xx} + \alpha_{yy} + \alpha_{zz}}{3}$$

$$\Delta\alpha = \frac{1}{\sqrt{2}}\sqrt{(\alpha_{xx} - \alpha_{yy})^2 + (\alpha_{yy} - \alpha_{zz})^2 + (\alpha_{zz} - \alpha_{xx})^2 + 6\left(\alpha_{xy}^2 + \alpha_{yz}^2 + \alpha_{xz}^2\right)}$$

The NLO results are given in Table 10. The calculated values were converted into electrostatic units (esu) from atomic units (a.u.) (for α, 1a.u = 0.1482×10^{-24} esu; for β, 1a.u = 8.6393×10^{-33} esu) [79]. The calculated values of μ, α and β are 6.0 D, $-23{,}7 \times 10^{-24}$ esu and $2577{,}1 \times 10^{-33}$ esu, respectively. The μ and β values obtained are very large (4.3 times for dipole moment, 7.5 times for hyperpolarizability) compared to that of urea (μ = 1.3732D, β = 343.272×10^{-33} esu) found in the literature [49]). Urea is the reference molecule which is used in the study of the NLO properties of molecular systems. Hence our results indicate that AQ is an effective candidate for NLO application.

3.11. Thermodynamic properties

Thermodynamic properties, including heat capacity (C_v), entropy (S) and enthalpy changes (ΔH) for title compound were also performed in the gas phase. The calculated properties are given in Table 11. From Tables 11 and it can be observed that these thermodynamic functions are increasing with temperature in the range 100–700K probably owing to the intensities of the molecular vibrations increasing with temperature [80,81]. The correlations between heat capacity, entropy, enthalpy changes and temperatures were fitted by quadratic formulars and the corresponding fitting factors (R^2) for these thermodynamic properties are 0.9992, 1.0000 and 0.9998 respectively. The corresponding fitting equations are defined as follows and the correlation graphics are shown in Fig. 8 (see Table 12).

$$C_v = 2.09229 + 0.34179T - 1.33345.10^{-4}T^2\ (R^2 = 0.9992)$$

$$S = 66.96 + 0.36384T - 7.95821.10^{-5}T^2\ (R^2 = 1.0000)$$

$$\Delta H = -1.12985 + 0.02069T + 1.1955.10^{-4}T^2\ (R^2 = 0.9998)$$

These thermodynamic data supply helpful information for the further study of AQ (see Fig. 9). They can be used to compute other thermodynamic energies based on the relationships between thermodynamic functions and estimate directions of chemical reactions

Table 9
NBO charges of AQ.

Atom	Charge	Atom	Charge	Atom	Charge	Atom	Charge	Atom	Charge
C1	−0.31742	C11	−0.04358	H21	0.2021	H31	0.16994	C41	−0.17653
C2	0.23772	C12	−0.20917	C22	0.32513	C32	−0.16437	H42	0.19451
C3	−0.10991	H13	0.23314	C23	−0.06542	H33	0.18977	H43	0.18977
C4	0.18213	H14	0.22383	C24	−0.19474	H34	0.15699	C44	−0.60113
C5	0.09398	Cl 15	0.00167	H25	0.21561	C35	−0.5822	H45	0.19497
H6	0.19659	N16	−0.48485	C26	0.12217	H36	0.20374	H46	0.20355
H7	0.22158	N17	−0.55906	C27	−0.2021	H37	0.19173	H47	0.19247
C8	−0.18579	N18	−0.6008	H28	0.20834	H38	0.20226		
C9	−0.19446	H19	0.38667	C29	−0.1821	O39	−0.66802		
H10	0.18292	C20	−0.26409	H30	0.21513	H40	0.46741		

Table 10
Second order perturbation theory analysis of Fock matrix in NBO basis for AQ.

Donor NBO (i)	Acceptor NBO (j)	E(2)a kcal.mol-1	E(*j*)-E(i)b a.u.	F(i,j)c a.u.
BD (1) C8 – C12	RY*(5) C44	10633.52	0.08	0.809
BD (1) N17 – C41	RY*(1) H30	9940.26	0.03	0.526
	BD*(1) C4–N16	50613.15	0.06	1.503
BD (1) C20 – C22	RY*(9) C24	41897.58	0.10	1.854
	RY*(4) H46	9895.59	0.29	1.531
BD (1) C22–O39	RY*(1) H31	52218.60	0.01	0.745
BD (1) C24–H25	RY*(7) C26	65072.77	0.03	1.336
	BD*(1) C4–C9	11211.72	0.10	0.957
	RY*(1) C24	92845.91	0.06	2.042
	RY*(7) C41	59862.22	0.10	2.139
BD (1) O39 – H40	RY*(4) H25	17618.20	0.34	2.193
	BD*(1) C11–C12	15939.07	0.24	1.749
	RY*(5) C41	15537.24	0.32	2.003
	BD*(1) C26–C27	14904.98	0.26	1.757
	RY*(9) C24	13286.74	0.41	2.093
	BD*(1) C4–N16	9843.83	0.37	1.696
CR (1) C41	RY*(17) C44	9604.83	0.47	1.896
CR (1) C44	RY*(17) C44	28780.08	0.43	3.142

Table 11
The electric dipole moment, polarizability and first order hyperpolarizability of AQ.

	a.u	esu (10^{-24})		a.u	esu (10^{-33})
α_{xx}	−176.8	−26.2	β_{xxx}	−197.4	−1705,6
α_{xy}	−2.1	−0.3	β_{xxy}	33.9	293,0
α_{yy}	−147.8	−21.9	β_{xyy}	−64.7	−558,8
α_{xz}	−8.5	−1.3	β_{yyy}	49.8	430,7
α_{yz}	−4.9	−0.7	β_{xxz}	−21.9	−189,3
α_{zz}	−155.4	−23.0	β_{xyz}	8.7	74,9
α	−160.0	−23.7	β_{yyz}	−25.6	−220,9
$\Delta\alpha$	31.3	4.6	β_{xzz}	−13.1	−112,8
μ_x	−4.8		β_{yzz}	7.9	67,9
μ_y	2.3		β_{zzz}	−22.4	−193,3
μ_z	−2.7		β_x	−275.2	−2377,1
μ	6.0		β_y	91.6	791,6
			β_z	−69.8	−603,4
			β	298.3	2577,1

according to the second law of thermodynamics [82].

4. Conclusion

In this study, when clarifying the characterization of AQ, structural parameters, vibrational frequencies, chemical shift values and UV spectra were calculated experimental and theoretical approaches were used to analyse structural and vibrational (FT-IR, ^{1}H and ^{13}C NMR and UV–visible) features of the AQ molecule. The calculations were performed using DFT method at the B3LYP/6–311++(d, p) level of theory then compared with corresponding experimental values. The geometrical parameters of the title compound agree with the XRD results given in literature. On basis of calculated potential energy distribution results assignments of the fundamental

Table 12
Thermodynamic functions of AQ at the B3LYP/6–311++G(d,p) level.

Temperature (K)	Heat capacities Cv(cal.mol^{-1}.k^{-1})	Entropies S (cal.mol^{-1}.k^{-1})	ΔH (Kcal/mol)
100	36.259	102.201	2388
200	63.607	137.137	7585
300	91.375	168.968	15,529
400	117.977	199.536	26,218
500	140.914	228.847	39,397
600	159.740	256.624	54,660
700	175.094	282.747	71,626

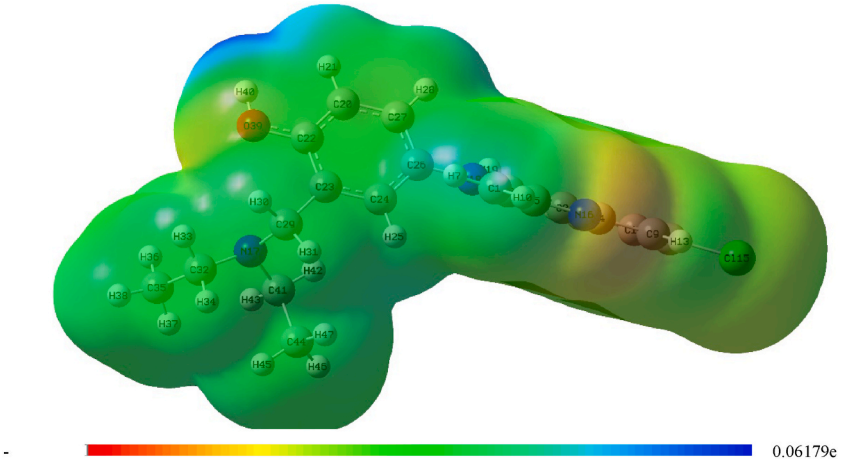

Fig. 8. Molecular electrostatic potential map of AQ.

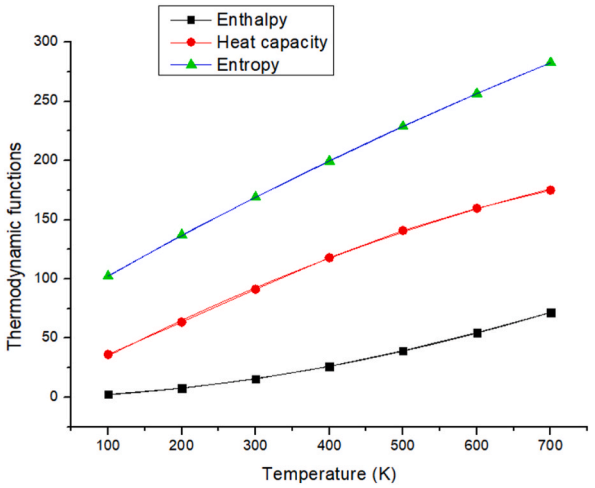

Fig. 9. Correlation graph of thermodynamic functions for AQ.

vibrational frequencies have been made unambiguously using VEDA program. A very good correlation between the observed and calculated vibrational spectra reveals the advantages of higher basis sets for quantum chemical calculations. ^{1}H and ^{13}C NMR calculations were done using GIAO methods and the results were found to be in good agreement with experimental data. The electronic properties were also simulated and compared with experimental UV–visible spectrum which exhibits mainly $\pi \rightarrow \pi^*$ and $n \rightarrow \pi^*$ absorption peaks. The calculated HOMO and LUMO energies reflected the charge transfer within the molecule. The mapped MEP surface support the electrophilic sites on positive charges of hydrogen atom of hydroxyl and amino groups while the nucleophilic sites are observed on the oxygen and nitrogen (N16) atoms. Stability of the molecule arising from hyper-conjugative interactions should lead to its bioactive's properties. Charge delocalization has been analyzed using NBO analysis. A computation of the first order

hyperpolarizability indicates that the title compound might be a good candidate as a NLO material.

5. Data availability

- No data associated with this study has been deposited into a publicly available repository.
- No data was used for the research described in the article.

CRediT authorship contribution statement

Pélagie Manwal A Mekoung: Writing – review & editing, Writing – original draft, Investigation, Formal analysis, Conceptualization. **Alhadji Malloum:** Methodology, Data curation. **Munusamy Govindarajan:** Visualization, Resources. **Rose Ngono Mballa:** Resources, Project administration. **Issofa Patouossa:** Visualization, Software, Formal analysis. **Auguste Abouem A Zintchem:** Formal analysis. **Charles P.N. Nanseu:** Investigation, Formal analysis. **Ibrahim N. Mbouombouo:** Writing – review & editing, Supervision, Project administration, Formal analysis, Conceptualization.

Declaration of competing interest

The authors declare that they have no known competing financial interests or personal relationships that could have appeared to influence the work reported in this paper.

Acknowledgement

The authors thank the University of Yaoundé I and the Higher Teacher Training College of Yaoundé (Cameroon) for infrastructural facilities.The authors are also grateful to the Head Director of the National Drug Quality Control and Valuation Laboratory, Yaoundé-Cameroon for providing laboratory facilities and spectral data.

References

[1] S. Rajabalian, A. Foroumadi, A. Shafiee, S. Emami, Functionalized N(2-oxyiminoethyl) piperazinyl quinolones as new cytotoxic agents, J Pharm Pharm Sci 10 (2007) 153–158.
[2] G.A.R.Y. Suaifan, A.A.M. Mohammed, B.A. Alkhawaja, Fluoroquinolones' biological activities against laboratory microbes and cancer cell lines, Molecules 27 (2022) 1658, https://doi.org/10.3390/molecules27051658.
[3] A.V. Shindikar, C.L. Viswanathan, Novel fluoroquinolones: design, synthesis, and in vivo activity in mice against Mycobacterium tuberculosis H37Rv, Bioorg. Med. Chem. Lett 15 (2005) 1803–1806, https://doi.org/10.1016/j.bmcl.2005.02.037.
[4] R.-H. Guo, Q. Zhang, Y.-B. Ma, X.-Y. Huang, J. Luo, L.-J. Wang, C.-A. Geng, X.-M. Zhang, J. Zhou, Z.-Y. Jiang, J.-J. Chen, Synthesis and biological assay of 4-aryl-6-chloro-quinoline derivatives as novel non-nucleoside anti-HBV agents, Bioorg. Med. Chem. 19 (2011) 1400–1408, https://doi.org/10.1016/j.bmc.2011.01.006.
[5] M. Yousuf, D. Mukherjee, A. Pal, S. Dey, S. Mandal, C. Pal, S. Adhikari, Synthesis and biological evaluation of ferrocenylquinoline as a potential antileishmanial agent, ChemMedChem 10 (2015) 546–554, https://doi.org/10.1002/cmdc.201402537.
[6] S. Guglielmo, M. Bertinaria, B. Rolando, M. Crosetti, R. Fruttero, V. Yardley, S.L. Croft, A. Gasco, A new series of amodiaquine analogues modified in the basic side chain with in vitro antileishmanial and antiplasmodial activity, Eur. J. Med. Chem. 44 (2009) 5071–5079, https://doi.org/10.1016/j.ejmech.2009.09.012.
[7] Y.-L. Chen, Y.-L. Zhao, C.-M. Lu, C.-C. Tzeng, J.-P. Wang, Synthesis, cytotoxicity, and anti-inflammatory evaluation of 2-(furan-2-yl)-4-(phenoxy)quinoline derivatives. Part 4, Bioorg. Med. Chem. 14 (2006) 4373–4378, https://doi.org/10.1016/j.bmc.2006.02.039.
[8] S. Bawa, S. Kumar, S. Drabu, R. Kumar, Structural modifications of quinoline-based antimalarial agents: recent developments, J Pharm Bioall Sci 2 (2010) 64, https://doi.org/10.4103/0975-7406.67002.
[9] J.H. Burckhalter, F.H. Tendick, E.M. Jones, P.A. Jones, W.F. Holcomb, A.L. Rawlins, Aminoalkylphenols as antimalarials. II. [1] (Heterocyclic-amino)-α-amino-o-cresols. The synthesis of camoquin [2], J. Am. Chem. Soc. 70 (1948) 1363–1373, https://doi.org/10.1021/ja01184a023.
[10] P. Olliaro, C. Nevill, J. LeBras, P. Ringwald, P. Mussano, P. Garner, P. Brasseur, Systematic review of amodiaquine treatment in uncomplicated malaria, Lancet 348 (1996) 1196–1201, https://doi.org/10.1016/S0140-6736(96)06217-4.
[11] J.P. Gil, Amodiaquine pharmacogenetics, Pharmacogenomics 9 (2008) 1385–1390, https://doi.org/10.2217/14622416.9.10.1385.
[12] O. Raobela, V. Andriantsoanirina, D.G. Rajaonera, T.A. Rakotomanga, S. Rabearimanana, F. Ralinoro, D. Ménard, A. Ratsimbasoa, Efficacy of artesunate–amodiaquine in the treatment of falciparum uncomplicated malaria in Madagascar, Malar. J. 17 (2018) 284, https://doi.org/10.1186/s12936-018-2440-0.
[13] N. Durrani, T. Leslie, S. Rahim, K. Graham, F. Ahmad, M. Rowland, Efficacy of combination therapy with artesunate plus amodiaquine compared to monotherapy with chloroquine, amodiaquine or sulfadoxine-pyrimethamine for treatment of uncomplicated Plasmodium falciparum in Afghanistan, Trop. Med. Int. Health 10 (2005) 521–529, https://doi.org/10.1111/j.1365-3156.2005.01429.x.
[14] M. Adjuik, P. Agnamey, A. Babiker, S. Borrmann, P. Brasseur, M. Cisse, F. Cobelens, S. Diallo, J. Faucher, P. Garner, S. Gikunda, P. Kremsner, S. Krishna, B. Lell, M. Loolpapit, P.-B. Matsiegui, M. Missinou, J. Mwanza, F. Ntoumi, P. Olliaro, P. Osimbo, P. Rezbach, E. Some, W. Taylor, Amodiaquine-artesunate versus amodiaquine for uncomplicated Plasmodium falciparum malaria in African children: a randomised, multicentre trial, Lancet 359 (2002) 1365–1372, https://doi.org/10.1016/S0140-6736(02)08348-4.
[15] S.G. Staedke, M.R. Kamya, G. Dorsey, A. Gasasira, G. Ndeezi, E.D. Charlebois, P.J. Rosenthal, Amodiaquine, sulfadoxine/pyrimethamine, and combination therapy for treatment of uncomplicated falciparum malaria in Kampala, Uganda: a randomised trial, Lancet 358 (2001) 368–374, https://doi.org/10.1016/S0140-6736(01)05557-X.
[16] H. McIntosh, Chloroquine or amodiaquine combined with sulfadoxine-pyrimethamine for treating uncomplicated malaria, in: the Cochrane Collaboration, in: The Cochrane Database of Systematic Reviews (Complete Reviews), John Wiley & Sons, Ltd, Chichester, UK, 2001, p. CD000386, https://doi.org/10.1002/14651858.CD000386.
[17] L.K. Basco, A. Same-Ekobo, V.F. Ngane, M. Ndounga, T. Metoh, P. Ringwald, G. Soula, Therapeutic efficacy of sulfadoxine-pyrimethamine, amodiaquine and the sulfadoxine-pyrimethamine-amodiaquine combination against uncomplicated Plasmodium falciparum malaria in young children in Cameroon, Bull. World Health Organ. 80 (2002) 538–545.
[18] A. Semeniuk, A. Niedospial, J. Kalinowska-Tluscik, W. Nitek, B.J. Oleksyn, Molecular geometry of antimalarial amodiaquine in different crystalline environments, J. Mol. Struct. 875 (2008) 32–41, https://doi.org/10.1016/j.molstruc.2007.03.065.

[19] H.P. Yennawar, M.A. Viswamitra, Steric and rotational constraints in the X-ray structure of the antimalarial drug amodiaquine, Curr. Sci. 61 (1991) 39–43.
[20] L.B. Casabianca, A.C. de Dios, ^{13} C NMR study of the self-association of chloroquine, amodiaquine, and quinine, J. Phys. Chem. A. 108 (2004) 8505–8513, https://doi.org/10.1021/jp047361b.
[21] R.O. Arise, S.-N. Elizabeth, S.T. Farohunbi, M.O. Nafiu, A.C. Tella, Mechanochemical synthesis, in vivo anti-malarial and safety evaluation of amodiaquine-zinc complex, Acta Fac. Med. Naissensis 34 (2017) 221–233, https://doi.org/10.1515/afmnai-2017-0024.
[22] M.J. O'Neil, The Merck Index: an Encyclopedia of Chemicals, Drugs, and Biologicals, thirteenth ed., Merck, Whitehouse Station, N.J., 2001. http://catdir.loc.gov/catdir/toc/wiley041/2003267062.html. (Accessed 2 June 2023).
[23] PubChem, Amodiaquine. https://pubchem.ncbi.nlm.nih.gov/compound/2165. (Accessed 2 June 2023).
[24] G. Selvi, Comparison of Theoretical & Experimental Studies of 2-Oxo-4-Phenyl Quinoline, (n.d.).
[25] Spectroscopic investigation (FT-IR, FT-Raman, NMR and UV-Vis),Conformational stability, NBO and thermodynamic analysis of 1-(2-methoxyphenyl) piperazine and 1-(2-chlorophenyl) piperazine by DFT approach, Pharm. Anal. Acta 6 (2015), https://doi.org/10.4172/2153-2435.1000391.
[26] M. Hagar, H.A. Ahmed, G. Aljohani, O.A. Alhaddad, Investigation of some antiviral N-heterocycles as COVID 19 drug: molecular docking and DFT calculations, IJMS 21 (2020) 3922, https://doi.org/10.3390/ijms21113922.
[27] M. Arguelho, J. Alves, S. Ramos, V. Júnior, J. Pires, A. Beatriz, Electrochemical and theoretical evaluation of the interaction between DNA and amodiaquine. Evidence of the guanine adduct formation, Química Nova. 33 (2009) 1291–1296, https://doi.org/10.1590/S0100-40422010000600014.
[28] E. Cortes, E. Márquez, J.R. Mora, E. Puello, N. Rangel, A. De Moya, J. Trilleras, Theoretical study of the adsorption process of antimalarial drugs into acrylamide-base hydrogel model using DFT methods: the first approach to the rational design of a controlled drug delivery system, Processes 7 (2019) 396, https://doi.org/10.3390/pr7070396.
[29] A.D. Becke, Density-functional exchange-energy approximation with correct asymptotic behavior, Phys. Rev. A. 38 (1988) 3098–3100, https://doi.org/10.1103/PhysRevA.38.3098.
[30] C. Lee, W. Yang, R.G. Parr, Development of the Colle-Salvetti correlation-energy formula into a functional of the electron density, Phys. Rev. B 37 (1988) 785–789, https://doi.org/10.1103/PhysRevB.37.785.
[31] R. Dennington, T.A. Keith, J.M. Millam, GaussView 6.0. 16, Semichem Inc., Shawnee Mission, KS, USA, 2016.
[32] M.J. Frisch, G.W. Trucks, H.B. Schlegel, G.E. Scuseria, Ma Robb, J.R. Cheeseman, G. Scalmani, V. Barone, G.A. Petersson, H. Nakatsuji, Gaussian 16, Revision A. 03, Gaussian, Inc., Wallingford CT, 2016, p. 3.
[33] N.M. O'Boyle, A.L. Tenderholt, K.M. Langner, cclib: a library for package-independent computational chemistry algorithms, J. Comput. Chem. 29 (2008) 839–845, https://doi.org/10.1002/jcc.20823.
[34] M.H. Jamróz, Vibrational energy distribution analysis (VEDA): scopes and limitations, Spectrochim. Acta Mol. Biomol. Spectrosc. 114 (2013) 220–230, https://doi.org/10.1016/j.saa.2013.05.096.
[35] CCCBDB listing of precalculated vibrational scaling factors, (n.d.). https://cccbdb.nist.gov/vibscalejustx.asp (accessed July 5, 2023).
[36] S.P. Vijaya Chamundeeswari, E.R.J. Jebaseelan Samuel, N. Sundaraganesan, Theoretical and experimental studies on 2-(2-methyl-5-nitro-1-imidazolyl)ethanol, Eur. J. Chem. 2 (2011) 136–145, https://doi.org/10.5155/eurjchem.2.2.136-145.169.
[37] K. Wolinski, J.F. Hinton, P. Pulay, Efficient implementation of the gauge-independent atomic orbital method for NMR chemical shift calculations, J. Am. Chem. Soc. 112 (1990) 8251–8260, https://doi.org/10.1021/ja00179a005.
[38] R. Ditchfield, Self-consistent perturbation theory of diamagnetism, Mol. Phys. 27 (1974) 789–807, https://doi.org/10.1080/00268977400100711.
[39] K.N. Chethan Prathap, N.K. Lokanath, Three novel coumarin-benzenesulfonylhydrazide hybrids: synthesis, characterization, crystal structure, Hirshfeld surface, DFT and NBO studies, J. Mol. Struct. 1171 (2018) 564–577, https://doi.org/10.1016/j.molstruc.2018.06.022.
[40] P. Govindasamy, S. Gunasekaran, G.R. Ramkumaar, Natural bond orbital analysis, electronic structure and vibrational spectral analysis of N-(4-hydroxyl phenyl) acetamide: a density functional theory, Spectrochim. Acta Mol. Biomol. Spectrosc. 130 (2014) 621–633, https://doi.org/10.1016/j.saa.2014.03.065.
[41] B.H. Stuart, Infrared Spectroscopy: Fundamentals and Applications, first ed., Wiley, 2004 https://doi.org/10.1002/0470011149.
[42] N. Burcu Arslan, N. Ozdemir, O. Dayan, N. Dege, M. Koparır, P. Koparır, H. Muglu, Direct and solvent-assisted thione–thiol tautomerism in 5-(thiophen-2-yl)-1,3,4-oxadiazole-2(3H)-thione: experimental and molecular modeling study, Chem. Phys. 439 (2014) 1–11, https://doi.org/10.1016/j.chemphys.2014.05.006.
[43] V. Arjunan, S. Mohan, Fourier transform infrared and FT-Raman spectra, assignment, ab initio, DFT and normal co-ordinate analysis of 2-chloro-4-methylaniline and 2-chloro-6-methylaniline, Spectrochim. Acta Mol. Biomol. Spectrosc. 72 (2009) 436–444, https://doi.org/10.1016/j.saa.2008.10.017.
[44] K. Karrouchi, S.A. Brandán, Y. Sert, H. El-marzouqi, S. Radi, M. Ferbinteanu, M.E.A. Faouzi, Y. Garcia, M. Ansar, Synthesis, X-ray structure, vibrational spectroscopy, DFT, biological evaluation and molecular docking studies of (E)-N'-(4-(dimethylamino)benzylidene)-5-methyl-1H-pyrazole-3-carbohydrazide, J. Mol. Struct. 1219 (2020), 128541, https://doi.org/10.1016/j.molstruc.2020.128541.
[45] D. Lin-Vien, N.B. Colthup, W.G. Fateley, J.G. Grasselli, Aromatic and heteroaromatic rings, in: The Handbook of Infrared and Raman Characteristic Frequencies of Organic Molecules, Elsevier, 1991, pp. 277–306, https://doi.org/10.1016/B978-0-08-057116-4.50023-7.
[46] P.M.A. Mekoung, B.Y.G. Mountessou, M.B. Mbah, M. Signe, A.A.A. Zintchem, C.P.N. Nanseu, I.N. Mbouombouo, Vibrational spectroscopic investigations, electronic properties, molecular structure and quantum mechanical study of an antifolate drug: pyrimethamine, Comput. Chem. 10 (2022) 157–185, https://doi.org/10.4236/cc.2022.104008.
[47] N.B. Colthup, L.H. Daly, S.E. Wiberley, Introduction to Infrared and Raman Spectroscopy, third ed., Academic Press, Boston, 1990.
[48] S.D. Kanmazalp, M. Macit, N. Dege, Hirshfeld surface, crystal structure and spectroscopic characterization of (E)-4-(diethylamino)-2-((4-phenoxyphenylimino) methyl)phenol with DFT studies, J. Mol. Struct. 1179 (2019) 181–191, https://doi.org/10.1016/j.molstruc.2018.11.001.
[49] D. Sajan, J. Binoy, B. Pradeep, K. Venkata Krishna, V.B. Kartha, I.H. Joe, V.S. Jayakumar, NIR-FT Raman and infrared spectra and ab initio computations of glycinium oxalate, Spectrochim. Acta Mol. Biomol. Spectrosc. 60 (2004) 173–180, https://doi.org/10.1016/S1386-1425(03)00193-8.
[50] A Guide to the Complete Interpretation of Infrared Spectral of Organic Structures | Wiley, (n.d.). https://www.wiley.com/en-us/A+Guide+to+the+Complete+Interpretation+of+Infrared+Spectral+of+Organic+Structures-p-9780471939986 (accessed June 4, 2023).
[51] M. Kurt, M. Yurdakul, Ş. Yurdakul, Molecular structure and vibrational spectra of 3-chloro-4-methyl aniline by density functional theory and ab initio Hartree-Fock calculations, J. Mol. Struct.: THEOCHEM 711 (2004) 25–32, https://doi.org/10.1016/j.theochem.2004.07.034.
[52] E. Romano, L. Davies, S.A. Brandán, Structural properties and FTIR-Raman spectra of the anti-hypertensive clonidine hydrochloride agent and their dimeric species, J. Mol. Struct. 1133 (2017) 226–235, https://doi.org/10.1016/j.molstruc.2016.12.008.
[53] R.M. Silverstein, F.X. Webster, D.J. Kiemle, D.L. Bryce, Spectrometric Identification of Organic Compounds, 8 edition, Wiley, 2014.
[54] V. Krishnakumar, N. Prabavathi, Scaled quantum chemical calculations and FTIR, FT-Raman spectral analysis of 2-Methylpyrazine, Spectrochim. Acta Mol. Biomol. Spectrosc. 72 (2009) 743–747, https://doi.org/10.1016/j.saa.2008.11.012.
[55] V. Krishnakumar, R. Ramasamy, Density functional and experimental studies on the FT-IR and FT-Raman spectra and structure of 2,6-diamino purine and 6-methoxy purine, Spectrochim. Acta Mol. Biomol. Spectrosc. 69 (2008) 8–17, https://doi.org/10.1016/j.saa.2007.02.020.
[56] S. Miertuš, E. Scrocco, J. Tomasi, Electrostatic interaction of a solute with a continuum. A direct utilizaion of AB initio molecular potentials for the prevision of solvent effects, Chem. Phys. 55 (1981) 117–129, https://doi.org/10.1016/0301-0104(81)85090-2.
[57] A.V. Marenich, C.J. Cramer, D.G. Truhlar, Universal solvation model based on solute electron density and on a continuum model of the solvent defined by the bulk dielectric constant and atomic surface tensions, J. Phys. Chem. B 113 (2009) 6378–6396, https://doi.org/10.1021/jp810292n.
[58] S. Subashchandrabose, A.R. Krishnan, H. Saleem, V. Thanikachalam, G. Manikandan, Y. Erdogdu, I.R. Ft, F.T. Raman, NMR spectral analysis and theoretical NBO, HOMO–LUMO analysis of bis (4-amino-5-mercapto-1, 2, 4-triazol-3-yl) ethane by ab initio HF and DFT methods, J. Mol. Struct. 981 (2010) 59–70.
[59] S. Gunasekaran, R.A. Balaji, S. Kumeresan, G. Anand, S. Srinivasan, Experimental and theoretical investigations of spectroscopic properties of N-acetyl-5-methoxytryptamine, Can. J. Anal. Sci. Spectrosc. 53 (2008) 149–162.
[60] A.A. Abdulridha, M.A. AlboHayAllah, S.Q. Makki, Y. Sert, H.E. Salman, A.A. Balakit, Corrosion inhibition of carbon steel in 1 M H2SO4 using new Azo Schiff compound: electrochemical, gravimetric, adsorption, surface and DFT studies, J. Mol. Liq. 315 (2020), 113690, https://doi.org/10.1016/j.molliq.2020.113690.

[61] M.A. AlboHayAllah, A.A. Balakit, H.I. Salman, A.A. Abdulridha, Y. Sert, New heterocyclic compound as carbon steel corrosion inhibitor in 1 M H_2SO_4, high efficiency at low concentration: experimental and theoretical studies, J. Adhes. Sci. Technol. 37 (2023) 525–547, https://doi.org/10.1080/01694243.2022.2034588.
[62] B. Kosar, C. Albayrak, Spectroscopic investigations and quantum chemical computational study of (E)-4-methoxy-2-[(p-tolylimino)methyl]phenol, Spectrochim. Acta Mol. Biomol. Spectrosc. 78 (2011) 160–167, https://doi.org/10.1016/j.saa.2010.09.016.
[63] N.O. Obi-Egbedi, I.B. Obot, M.I. El-Khaiary, Quantum chemical investigation and statistical analysis of the relationship between corrosion inhibition efficiency and molecular structure of xanthene and its derivatives on mild steel in sulphuric acid, J. Mol. Struct. 1002 (2011) 86–96, https://doi.org/10.1016/j.molstruc.2011.07.003.
[64] T. Rajamani, S. Muthu, Vibrational spectra, first order hyperpolarizability, NBO, Fukui function and HOMO–LUMO analysis of 2-[4-(1,3-benzodioxol-5-ylmethyl)-1-piperazinyl] pyrimidine, Spectrochim. Acta Mol. Biomol. Spectrosc. 115 (2013) 654–666, https://doi.org/10.1016/j.saa.2013.06.040.
[65] D.A. Dhas, I.H. Joe, S.D.D. Roy, T.H. Freeda, DFT computations and spectroscopic analysis of a pesticide: chlorothalonil, Spectrochim. Acta Mol. Biomol. Spectrosc. 77 (2010) 36–44, https://doi.org/10.1016/j.saa.2010.04.020.
[66] M. Ríos-Gutiérrez, A. Saz Sousa, L.R. Domingo, Electrophilicity and nucleophilicity scales at different DFT computational levels, J of Physical Organic Chem 36 (2023), e4503, https://doi.org/10.1002/poc.4503.
[67] P.W. Ayers, R.G. Parr, Variational principles for describing chemical reactions: the Fukui function and chemical hardness revisited, J. Am. Chem. Soc. 122 (2000) 2010–2018, https://doi.org/10.1021/ja9924039.
[68] C. Morell, A. Grand, A. Toro-Labbe, Theoretical support for using the Δf(r) descriptor, Chem. Phys. Lett. 425 (2006) 342–346, https://doi.org/10.1016/j.cplett.2006.05.003.
[69] W. Guerrab, I.-M. Chung, S. Kansiz, J.T. Mague, N. Dege, J. Taoufik, R. Salghi, I.H. Ali, M.I. Khan, H. Lgaz, Y. Ramli, Synthesis, structural and molecular characterization of 2,2-diphenyl-2H,3H,5H,6H,7H-imidazo[2,1-b][1,3]thiazin-3-one, J. Mol. Struct. 1197 (2019) 369–376, https://doi.org/10.1016/j.molstruc.2019.07.081.
[70] S. Demir, S. Cakmak, N. Dege, H. Kutuk, M. Odabasoglu, R.A. Kepekci, A novel 3-acetoxy-2-methyl-N-(4-methoxyphenyl)benzamide: molecular structural describe, antioxidant activity with use X-ray diffractions and DFT calculations, J. Mol. Struct. 1100 (2015) 582–591, https://doi.org/10.1016/j.molstruc.2015.08.014.
[71] S. Kansız, N. Dege, Synthesis, crystallographic structure, DFT calculations and Hirshfeld surface analysis of a fumarate bridged Co(II) coordination polymer, J. Mol. Struct. 1173 (2018) 42–51, https://doi.org/10.1016/j.molstruc.2018.06.071.
[72] E.D. Glendening, A.E. Reed, J.E. Carpenter, F. Weinhold, NBO, Gaussian, Inc., Pittsburgh, PA, 2003 version 3.1.
[73] H.A. Khamees, M. Jyothi, S.A. Khanum, M. Madegowda, Synthesis, crystal structure, spectroscopic characterization, docking simulation and density functional studies of 1-(3, 4-dimethoxyphenyl)-3-(4-flurophenyl)-propan-1-one, J. Mol. Struct. 1161 (2018) 199–217.
[74] N. Mallem, D. Khatmi, S. Azzouz, S. Benghodbane, O.A. Yahia, Computational studies of 1: 2 complex between retinol propionate and β cyclodextrin, J. Inclusion Phenom. Macrocycl. Chem. 73 (2012) 305–312.
[75] M. Evecen, H. Tanak, F. Tinmaz, N. Dege, İ. Ozer İlhan, Experimental (XRD, IR and NMR) and theoretical investigations on 1-(2-nitrobenzoyl)3,5-bis(4-methoxyphenyl)-4,5-dihydro-1H-pyrazole, J. Mol. Struct. 1126 (2016) 117–126, https://doi.org/10.1016/j.molstruc.2016.01.069.
[76] E. Huo, S. Shahab, S.A. Saud, W. Cheng, P. Lu, M. Sheikhi, R. Alnajjar, S. Kaviani, Quantum chemical modeling, synthesis, spectroscopic (FT-IR, excited States, UV–Vis) studies, FMO, QTAIM, NBO and NLO analyses of two new azo derivatives, J. Mol. Struct. 1243 (2021), 130810, https://doi.org/10.1016/j.molstruc.2021.130810.
[77] D.F. Eaton, Nonlinear optical materials, Science 253 (1991) 281–287, https://doi.org/10.1126/science.253.5017.281.
[78] Y.-X. Sun, Q.-L. Hao, W.-X. Wei, Z.-X. Yu, L.-D. Lu, X. Wang, Y.-S. Wang, Experimental and density functional studies on 4-(3,4-dihydroxybenzylideneamino) antipyrine, and 4-(2,3,4-trihydroxybenzylideneamino)antipyrine, J. Mol. Struct.: THEOCHEM 904 (2009) 74–82, https://doi.org/10.1016/j.theochem.2009.02.036.
[79] J. Prashanth, G. Ramesh, J.L. Naik, J.K. Ojha, B.V. Reddy, G.R. Rao, Molecular structure, vibrational analysis and first order hyperpolarizability of 4-methyl-3-nitrobenzoic acid using density functional theory, OPJ 5 (2015) 91–107, https://doi.org/10.4236/opj.2015.53008.
[80] Chemical Thermodynamics: Advanced Applications - first ed., (n.d.). https://shop.elsevier.com/books/chemical-thermodynamics-advanced-applications/bath/978-0-12-530985-1 (accessed June 5, 2023).
[81] D. Shoba, S. Periandy, M. Govindarajan, P. Gayathri, Spectroscopic and quantum chemical analysis of Isonicotinic acid methyl ester, Spectrochim. Acta Mol. Biomol. Spectrosc. 136 (2015) 852–863, https://doi.org/10.1016/j.saa.2014.09.104.
[82] R. Zhang, B. Du, G. Sun, Y. Sun, Experimental and theoretical studies on o-, m- and p-chlorobenzylideneaminoantipyrines, Spectrochim. Acta Mol. Biomol. Spectrosc. 75 (2010) 1115–1124, https://doi.org/10.1016/j.saa.2009.12.067.